The Astrophysical Journal, 991:5 (7pp), 2025 September 20 https://doi.org/10.3847/1538-4357/adfa8c

Ultraviolet and Gravitational Wave Signatures of Magnetar Formation

Simone Dall'Osso[1] and Dafne Guetta[2]
[1] INAF—Istituto di Radioastronomia, via Gobetti 101, Bologna, 40129, Italy; simone.dallosso@inaf.it
[2] Physics Department, Ariel University, Ariel, Israel
Received 2025 April 30; revised 2025 August 9; accepted 2025 August 9; published 2025 September 11

Abstract

We investigate the impact of gravitational wave (GW) emission by a newly born magnetar onto its electromagnetic (EM) counterparts in the Ultraviolet Transient Astronomy Satellite (ULTRASAT) band. In particular, we carry out a numerical calculation of magnetar-powered shock breakouts (SBOs) and supernova (SN) light curves. We find that an early SBO peak in the bolometric light curves provides a likely signature of a magnetar central engine, which can help constrain the magnetar's spin period and magnetic dipole. Moreover, our results show that GW emission by the magnetar has only a minor effect on the SBO light curve. Such SBOs can be detected by ULTRASAT at a rate $\sim$1–2 yr^{-1}, provided that the magnetar wind is not efficiently thermalized during the early phases of the evolution. We additionally find that the subsequent SN light curves can be more luminous than SBOs in the ULTRASAT band and can thus be detected at a higher rate. Finally, we find a possible late-time signature of GW emission in the SN light curves, which may provide an additional tool for the detection of GW signals. Our results demonstrate that future ULTRASAT observations will provide crucial insights into the magnetar formation process and unique information for direct searches of long-transient signals with current and future generation GW detectors. In particular, we estimate a rate of multimessenger (UV+GW) detections of newly formed magnetars $\gtrsim$1 every 2 yr with ULTRASAT and the Einstein Telescope.

Unified Astronomy Thesaurus concepts: Magnetars (992); Ultraviolet astronomy (1736)

1. Introduction

The study of explosive transients associated to cosmic cataclysmic events has been a major focus of time domain astronomy in the last decade, with many dedicated surveys—e.g. Zwicky Transient Facility (ZTF), EUCLID, eROSITA, and the Vera Rubin Observatory—and a wealth of new discoveries. Several such transients are expected to have a significant component of emission in the UV band (I. Sagiv et al. 2014; S. Kulkarni et al. 2021), which has been historically poorly covered in the broadband monitoring of astrophysical transients. The Ultraviolet Transient Astronomy Satellite (ULTRASAT) is a small mission dedicated to time domain observations in the near-UV (NUV) band; scheduled to launch in 2026, it will carry out the first wide-field survey of transient and variable sources, with a much improved sensitivity relative to previous UV detectors. One of the main science cases for ULTRASAT is the early (hr) detection of core-collapse supernovae (CCSNe) and the high-cadence (minutes) monitoring of their UV light curves. Approximately 10% of CCSNe are expected to form magnetars (B. M. Gaensler et al. 2005; P. Beniamini et al. 2019), highly magnetized neutron stars (NS) that are thought to be formed with millisecond spin periods and huge interior magnetic fields (>several $\times 10^{15}$ G). Due to these extreme conditions, a newly formed magnetar will be able to release in the surrounding environment large amounts of energy ($>10^{51}$–10^{52} erg) in short timescales (<a few hr), in the electromagnetic (EM) and/or gravitational wave (GW) channels. Therefore, these objects are considered to be prime candidates for multi-messenger studies of NS astrophysics (e.g., B. Zhang & P. Mészáros 2001; C. Cutler 2002; S. Dall'Osso et al. 2009, 2015, 2018; B. P. Gompertz et al. 2014, 2015; S. Lander & D. Jones 2020; S. Dall'Osso & L. Stella 2022; O. Gottlieb & B. D. Metzger 2024; G. P. Lamb et al. 2025; H. Sun et al. 2025).

In S. S. Menon et al. (2023; hereafter Paper I) we considered magnetar-driven shock breakouts (SBOs), a specific signature of newly born magnetars (D. Kasen & L. Bildsten 2010; G. Leloudas et al. 2012; M. Nicholl et al. 2015; D. Kasen et al. 2016; L.-D. Liu et al. 2021; S. S. Menon et al. 2023), particularly relevant in the ULTRASAT band. In that work we adopted approximate power-law solutions for the evolution of the SBO physics properties (e.g., radius, velocity, pressure) and corresponding approximate expressions for the expected SBO luminosity in order to estimate the detectability and rate of these transients with ULTRASAT. Here we extend that study to calculate exact numerical solutions for the SBO evolution and its luminosity. Moreover, we account for the possibility of significant GW emission from newly born magnetars, which will reduce the available energy in the EM channel, directly impacting the shock dynamics and its observational signatures, e.g., the SBO. Additionally, we calculate the supernova (SN) light curve that follows the SBO and that is similarly affected by energy injection from the magnetar central engine and by the potential GW emission (e.g., J. Greiner et al. 2015; L. Xie et al. 2024).

GW signals from newly born magnetars are expected to be stronger than those from the core collapse itself, making them detectable at greater distances (S. Dall'Osso & L. Stella 2022 and references therein). This enhances the importance of directed searches for magnetar-driven GW signals, particularly during the future O5 science run of advanced GW detectors (LIGO-Virgo-KAGRA), as well as the planned third-generation detectors (Einstein Telescope and Cosmic Explorer). Because SBOs occur at early times after the explosion and

prior to SNe, they will serve as well-defined triggers for directed GW searches (as well as for other EM follow-up observations) and will contribute to enhancing the search sensitivity.

We have organized the paper as follows. In Section 2 we summarize the main properties of magnetar-driven SBOs and extend the definitions of various physical quantities to allow for a generalization of the model. In Section 3 we introduce the GW emission term and calculate its impact on the SBO physics. In Section 4 we describe the model for SN light curves, including the effect of inefficient thermalization of the magnetar power. In Section 5 we calculate the bolometric and UV light curves expected from magnetar-driven SBOs and SNe with and without GW emission and evaluate the detection horizon with ULTRASAT. For comparison, we also evaluate the ZTF horizon for our model. In Section 6 we calculate the expected detection rate with ULTRASAT of both magnetar-driven SBOs and their associated SN light curves. Finally, in Section 7 we discuss our results, emphasizing their many astrophysical implications.

2. Magnetar-driven SBO Light Curves

A newly born millisecond spinning magnetar, with angular velocity $\Omega = 2\pi/P$ and moment of inertia I, has the rotational energy

$$E_{\rm m} = \frac{1}{2} I\Omega^2 \approx 3 \times 10^{52} \quad {\rm erg} \quad P_{\rm ms}^{-2} M_{1.4} R_{12}^2, \tag{1}$$

expressing the spin period in milliseconds, the mass in units of 1.4 $M_\odot$, and setting the radius $R = 12$ km. The NS spins down due to magnetic dipole radiation on a timescale t_m (defined in Equation (2) of Paper I), releasing rotational energy at the rate L_m (see, e.g., Paper I).

The energy is released in the form of an MHD wind, which inflates a high-pressure bubble of relativistic particles and magnetic field that sweeps the previously launched SN ejecta into a thin shell of radius r_s, driving a shock through it. The density profile within the ejecta can be approximated by a broken power law, which is shallow in the inner region and becomes very steep close to the surface (D. Kasen et al. 2016 and references therein):

$$\rho(r, t) = \begin{cases} \zeta_\rho \frac{M_{\rm SN}}{v_t^3 t^3} \left(\frac{r}{t v_t}\right)^{-\delta} & \text{if } r/t < v_t \\ \zeta_\rho \frac{M_{\rm SN}}{v_t^3 t^3} \left(\frac{r}{t v_t}\right)^{-n} & \text{if } r/t \geqslant v_t, \end{cases} \tag{2}$$

where the transition occurs at the velocity coordinate

$$v_t \approx 3 \times 10^8 \ {\rm cm\ s^{-1}} \zeta_v \left(\frac{E_{\rm SN,\,51}}{M_{\rm SN}/5M_\odot}\right)^{1/2} \tag{3}$$

for a homologous expansion of the shell. Typical values are $\delta = 1$ and $n = 10$ for CCSNe (R. A. Chevalier & N. Soker 1989), while the two coefficients $\zeta_{v,\rho}$, of order unity, are given in D. Kasen et al. (2016).

Inside the shock, energy is dissipated at the rate $\dot{\epsilon}_{\rm sh}$

$$\dot{\epsilon}_{\rm sh} = 4\pi r_{\rm s}^2 \frac{\rho}{2} v_{\rm ej}^3 \eta^3, \tag{4}$$

where $v_{\rm ej} = r_{\rm s}/t$ is the velocity of the ejecta at the shell radius $r_{\rm s}$ and η is the shock strength parameter

$$\eta(t) = \frac{v_{\rm s} - v_{\rm ej}}{v_{\rm ej}} = \frac{t}{r_{\rm s}} \left(\frac{dr_{\rm s}}{dt} - \frac{r_{\rm s}}{t}\right), \tag{5}$$

v_s being the shock velocity, i.e., dr_s/dt.

In Paper I we adopted approximate power-law solutions for r_s and v_s (and the bubble pressure, p_B), assuming the magnetar spins down only due to magnetic dipole radiation. However, such solutions may not apply in a more general case in which an additional torque, e.g., GW emission, contributes to the magnetar spindown. Moreover, both the shock heating rate (Equation (4)) and the SBO luminosity (Equation (24) in D. Kasen et al. 2016) scale as η^3, and therefore an accurate determination of the shock strength is crucial, even when only magnetic dipole radiation is involved. We thus turned to a numerical solution of the mass, momentum, and energy equations in the shock (R. A. Chevalier 2005) in order to determine the exact time evolution $r_{\rm s}(t)$, $v_s(t)$, and $v_{\rm ej}$ under general conditions, from which a numerical expression for $\eta(t)$ was derived.

SBO occurs when the shock becomes radiative upon reaching the region within the ejecta where the photon optical depth $\tau \approx c/v_s$. The breakout radius, $r_{\rm bo}$, is thus calculated from the ejecta structure (Equation (2)), setting

$$\tau(r_{\rm bo}, t) = \kappa \int_{r_{\rm bo}}^{+\infty} \rho(r, t) dr = c/v_s(t), \tag{6}$$

where the opacity $\kappa \approx 0.1$ cm^2 g^{-1}.

Equation (6) allows to calculate at once $r_{\rm bo}$ and the breakout time, $t_{\rm bo}$, for a given solution $r_s(t)$. The resulting bolometric luminosity is (D. Kasen et al. 2016)

$$L_{\rm sbo}(t) \approx e^{-\left(\frac{t}{t_{\rm bo}}\right)^2} \int_0^t 2\dot{\epsilon}_{sh}(t') \frac{t'}{t_{\rm bo}^2} e^{-\left(\frac{t'}{t_{\rm bo}}\right)^2} dt'. \tag{7}$$

Finally, radiation produced at SBO will be released at the (outer) photospheric radius, $r_{\rm ph}$, where the scattering optical depth equals unity, i.e., $r_{\rm ph}$ is determined by a similar expression as Equation (6), imposing that the l.h.s. = 1. Because of such conditions, the resulting radiation spectrum at breakout will be very closely approximated by a blackbody of radius $r_{\rm ph}$ and effective temperature $T_{\rm bb}^4 = L_{\rm sbo}/(\sigma 4\pi r_{\rm ph}^2)$, where both the luminosity and the photospheric radius (hence the blackbody temperature) are functions of time.

3. Effects of GW Emission

The birth parameters of magnetars are still widely discussed in the literature. The currently leading scenario suggests that their strong B-field is a consequence of very fast rotation at birth—a few milliseconds at most—which sustains a powerful dynamo action (R. C. Duncan & C. Thompson 1992; V. V. Usov 1992; C. Thompson & R. C. Duncan 1993; R. Raynaud et al. 2020; see, however, L. Ferrario & D. Wickramasinghe 2006; J. Vink & L. Kuiper 2006; J. Vink 2008). The combination of a very strong magnetic field and extreme rotation implies favorable conditions for strong GW emission (C. Cutler 2002; L. Stella et al. 2005; S. Dall'Osso et al. 2009, 2015, 2018; S. Lander & D. Jones 2020; S. Dall'Osso & L. Stella 2022), which in turn implies important modifications of the equations for the shock evolution and therefore of the SBO luminosity and detectability.

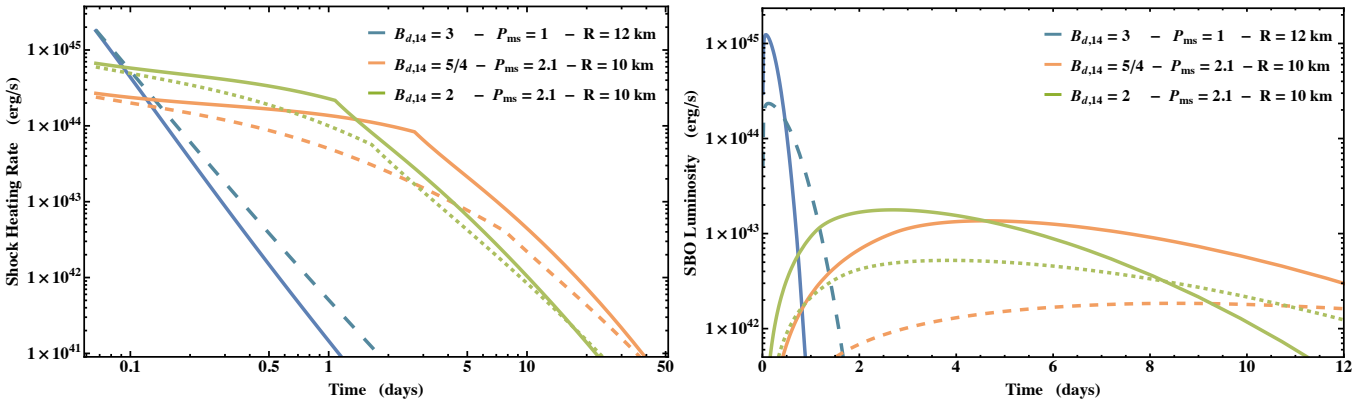

Figure 1. Left panel: shock heating rate, $\dot{\epsilon}_{sh}$ vs. time (Equation (4)) for fiducial parameter values of the SN ejecta ($E_{SN} = 10^{51}$ erg, $M_{SN} = 5M_{\odot}$) and three sets of (P, B, R)-values for the magnetar central engine, as indicated in the legend. Right panel: bolometric SBO light curve (Equation (7)) for the same set of parameters as in the left panel. The dashed curves next to each of the solid curves in both panels (long dashing for the blue curve, upper case in the legend; medium dashing for the orange curve, intermediate case in the legend; short dashing for the green curve, lower case in the legend) are obtained for the same magnetar parameters, adding the emission of GW with an ellipticity $\epsilon = 2 \times 10^{-3}$.

GW emission is caused by a deviation of the NS from spherical symmetry, which is parameterized in terms of a NS ellipticity, ϵ. GWs drain energy from the magnetar's spin and thus reduce the available power in the EM channel, i.e., the rate of energy injection in the shock. For a maximally emitting NS with ellipticity ϵ, moment of inertia I, and spin period P, the GW luminosity is

$$L_{GW} = \frac{32}{5}\frac{G}{c^5}(I\epsilon)^2\Omega^6, \tag{8}$$

and the total spindown luminosity of the NS is

$$I\Omega\dot{\Omega} = L_{EM} + L_{GW} = -\frac{\mu^2\Omega^4}{c^3} - \frac{32}{5}\frac{G}{c^5}(I\epsilon)^2\Omega^6. \tag{9}$$

By solving Equation (9) for Ω (the analytical solution was derived, e.g., in S. Dall'Osso et al. 2009 and H. Gao et al. 2016), we calculate the energy injection power, L_{EM}, in the MHD wind and the corresponding evolution of the shock parameters with GW emission included. Our results for the shock heating rate and SBO luminosity are reported in the panels of Figure 1 for models with (dashed curves) and without (solid curves) GW, for different choices of the NS spin period and magnetic dipole at birth, and a fixed $\epsilon = 2 \times 10^{-3}$ (chosen for illustration purposes). Any value of ϵ between zero and 2×10^{-3} would result in curves lying between the two extremes shown in our figures.

For the sake of our argument, we assume the NS ellipticity to be caused by a strong, interior magnetic field, B_{int}, according to the standard scaling (e.g., C. Cutler 2002)

$$\epsilon_B \sim 5 \times 10^{-4}(B_{in}/10^{16}\,\mathrm{G})^2. \tag{10}$$

However our calculations hold in general, regardless of the origin of the NS asphericity (see, e.g., A. Corsi & P. Mészáros 2009; A. Sur & B. Haskell 2021).

Figure 1 illustrates the time evolution of the shock heating rate (left panel, Equation (4)) and of the corresponding SBO bolometric luminosity (right panel, Equation (7)) for fiducial values of the SN ejecta ($M_{SN} = 5M_{\odot}$) and explosion energy ($E_{SN} = 10^{51}$ erg) for three different combinations of the NS spin and magnetic dipole field and for the case with (dashed curves) and without (solid curves) GW emission (fixed $\epsilon = 2 \times 10^{-3}$). In Figure 2 we show the corresponding evolution of η for the same combinations of NS parameters,

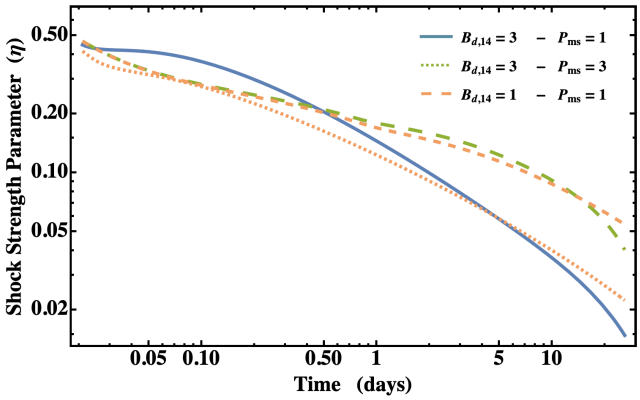

Figure 2. The shock strength parameter vs. time for four different combinations of the following NS parameters: (a) $B_{d,14} = 3$ and $P_{ms} = 1$; (b) $B_{d,14} = 5$ and $P_{ms} = 1$; (c) same as (a) with GW added; (d) same as (b) with GW added. In (c) and (d) GW emission is caused by an $\epsilon = 2 \times 10^{-3}$.

with/without GW emission. Figure 3 depicts t_{bo} versus (P, B_d) in the case without (left panel) and with (central panel) GW emission at a fixed $\epsilon = 2 \times 10^{-3}$ and for the same fiducial SN ejecta parameters. The right panel of Figure 3 shows instead t_{bo} contours as a function of (B_d, ϵ) at a fixed spin period of 1 ms.

4. Magnetar-driven SN Light Curves

The MHD bubble inflated by the magnetar also impacts the ejecta dynamics and, upon thermalization of the injected energy, the SN light curve. Such a scenario is frequently invoked to explain some properties of superluminous SNe (SLSNe; e.g., A. Gal-Yam 2019; T. J. Moriya 2024). Since the SN luminosity represents an energy sink in the evolution equation for the shock radius $r_s(t)$, it is a crucial ingredient for our model.

Here we calculate magnetar-powered SN light curves allowing for (i) GW emission from the central engine, as outlined in Section 3, and (ii) inefficient thermalization of the injected energy, which suppresses the early SN luminosity and lowers its peak. We then combine the SBO and SN light curves to estimate the expected detection rate with ULTRASAT of either type of transient and the prospects for

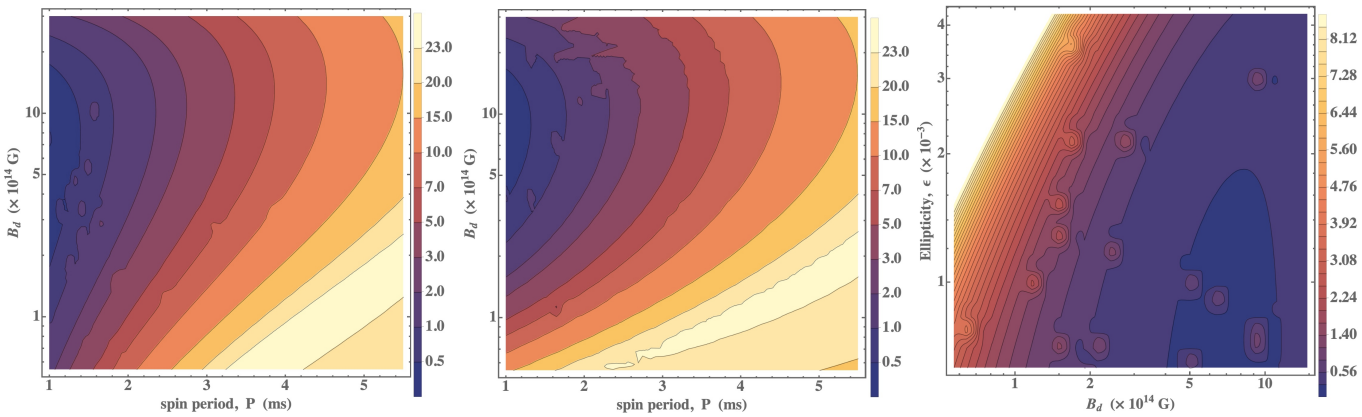

Figure 3. Breakout time, $t_{\rm bo}$ (in days), as a function of the magnetar parameters for fiducial values of the NS mass and radius (1.4 $M_\odot$ and 12 km, respectively) and of the SN explosion energy and ejecta mass (10^{51} erg and 5 $M_\odot$, respectively). Left panel: only magnetic dipole spindown, with no GW emission. Central panel: same as in the left panel but with GW-driven spindown added, adopting an ellipticity $\epsilon = 10^{-3}$. Right panel: magnetic dipole plus GW-driven spindown. Breakout time (in days) vs. B_d and ϵ (in units of 10^{-3}), for a fixed spin period of 1 ms.

multimessenger observations of newly formed magnetars with planned future facilities.

The SN light curve is calculated using the one-zone model presented in D. Kasen & L. Bildsten (2010) and D. Kasen et al. (2016) and the first principle of thermodynamics applied to the ejecta. Energy is lost due to adiabatic expansion (pdV work) and photon diffusion (SN luminosity), while the magnetar spindown power released in the EM channel, $L_{\rm EM}$, provides a continuous energy input. The spin energy lost to GWs, on the other hand, leaves the system without interacting with the ejecta.

The thermalization of $L_{\rm EM}$ within the ejecta takes a finite time, $t_{\rm th}$, prior to which it contributes to the ejecta dynamics but not to the SN emission (D. Kasen et al. 2016). During this time, the MHD wind energy is converted to $e^{\pm}$-pairs and high-energy photons ($\epsilon_\gamma \gg m_e c^2$) that, through a "pair cascade," lead to the formation of an optically thick nebula, quickly thermalizing a fraction $Y \sim 0.1$ of the MHD wind energy. The remaining fraction, $1 - Y$, is carried by a nonthermal component of high-energy photons, which are slowly thermalized via absorption by the nebula walls (the ejecta). The characteristic thermalization time is $t_{\rm th} = t_{\rm d}^{\rm n}/(1 - A)$, where A is the albedo of the ejecta and $t_{\rm d}^{\rm n} = (\tau_{\rm es} + 1) r_n/c$ the nebula crossing time for high-energy photons, determined by the scattering optical depth $\tau_{\rm es} = \sigma_T r_n n^{\pm}$, r_n being the radius of the nebula and $n^{\pm}$ the pair density.

The injection power effectively contributing to the SN emission is therefore expressed as (B. D. Metzger & A. L. Piro 2014)

$$L_{\rm eff}(t) = \frac{L_{\rm EM}(t)}{(1 + t/t_{\rm th})}, \tag{11}$$

and the following formal solution is obtained:

$$L_{\rm SN}(t) \approx e^{-\left(\frac{t}{t_{\rm sn}}\right)^2} \int_0^t 2 L_{\rm eff}(t') \frac{t'}{t_{\rm sn}^2} e^{-\left(\frac{t'}{t_{\rm sn}}\right)^2} dt'. \tag{12}$$

Here $t_{\rm sn} = \sqrt{(3\kappa M_{\rm ej})/(4\pi v_{\rm F} c)}$ is the effective photon diffusion time, $v_F = \sqrt{2(E_{\rm sn} + E_{\rm EM})/M_{\rm ej}}$ is the final ejecta velocity, and $E_{\rm EM} = \int L_{\rm EM}(t') dt'$ the total injected energy, including both the thermalized and nonthermalized component.

5. ULTRASAT Detection Horizon

Following Paper I we express the SBO/SN luminosities in the observed UV band, $L_{\rm sbo/SN}^{\rm UV}$, as a fraction f_{UV} of the corresponding bolometric luminosities, where

$$f_{UV} = \frac{\int_{\lambda_{\rm min}/(1+z)}^{\lambda_{\rm max}/(1+z)} B_\lambda(T_{\rm bb})\, d\lambda}{\sigma T_{\rm bb}^4}, \tag{13}$$

with B_λ the spectral radiance per unit wavelength. The blackbody temperature of either emission depends, through the bolometric luminosities $L_{\rm sbo/SN}$ and the photospheric radius, $r_{\rm ph}$, on the magnetar parameters (B, P, ϵ) as well as on the SN parameters ($E_{\rm SN}$, $M_{\rm SN}$). Note that, in Equation (13), the observed spectral range must be calculated taking into account the cosmological redshift. Thus, $f_{\rm UV}$ is a function of z as well as of the source physics parameters.

Figure 4 shows the predicted SBO+SN composite light curve in the ULTRASAT band for a particular set of NS parameters (1 ms spin period and $B_d = 2 \times 10^{14}$ G) and ideal thermalization efficiency (left) versus inefficient thermalization (right), without GW emission (solid curves) and with GW emission (dashed curves) for a fixed $\epsilon = 2 \times 10^{-3}$. The light curves were calculated for a source at redshift $z = 0.1$. We checked that the absolute luminosity in the ULTRASAT band has a weak dependence on redshift, at least up to $z = 0.5$. The plots show that the signature of the SBO is typically distinguishable from the SN in the bolometric light curves, while it is only visible in the UV band in the model with inefficient thermalization. Moreover, we find that the impact of GW emission can be significant over a wide parameter range, particularly on the SN evolution of the SN light curve, as further discussed in Section 7.

We also derive a maximum detection distance, $z_{\rm max}$, for either SBOs and SNe in the 230–290 nm band, given the ULTRASAT mean limiting magnitude of 22.5 ABmag (Y. Shvartzvald et al. 2024). Since the amount of extinction in the host galaxy is unknown a priori and is expected to present wide variations among different events, we adopt a (conservative) value of $A_{\rm NUV} \sim 2$ mag (N. Ganot et al. 2016). The resulting $z_{\rm max}$ is a function of (B, P, ϵ, $E_{\rm SN}$, $M_{\rm SN}$). We fixed the SN ejecta mass and explosion energy to the same fiducial parameters mentioned above and adopted the same

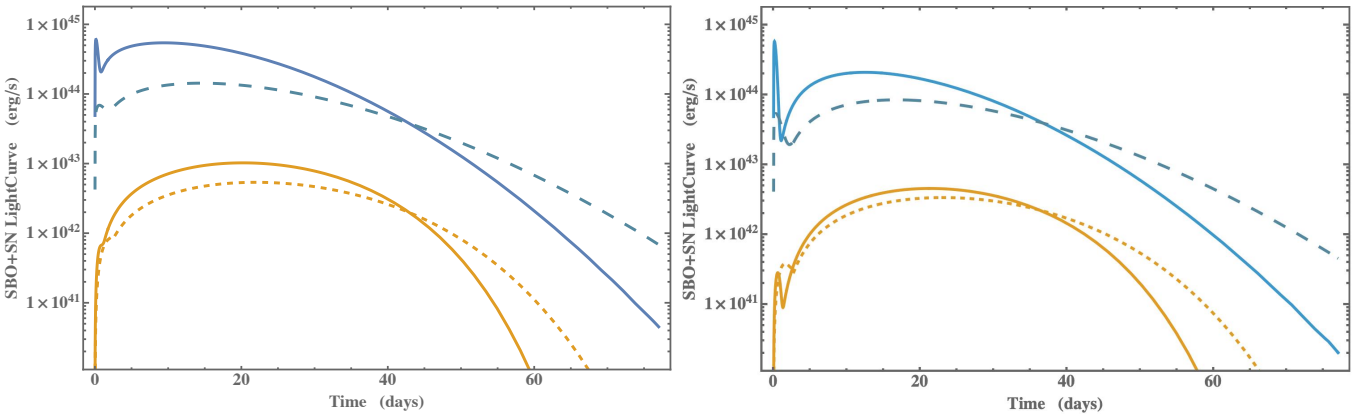

Figure 4. The composite light curves for the SBO + SN, bolometric (upper, blue), and in the ULTRASAT band (lower, orange) for $z = 0.1$ in the case with (dashed curves) and without (solid curves) GW emission ($\epsilon = 2 \times 10^{-3}$). Curves are drawn for $B_{d,14} = 2$ and $P_{\rm ms} = 1$ and fiducial values for other model parameters (see text). Left panel: the SN light curves were calculated assuming perfect thermalization of the magnetar spindown power within the ejecta. Right panel: inefficient thermalization of the magnetar spindown power within the ejecta was assumed (e.g., B. D. Metzger & A. L. Piro 2014) to calculate the SN light curves, with an albedo $A = 0.75$ for the ionized plasma.

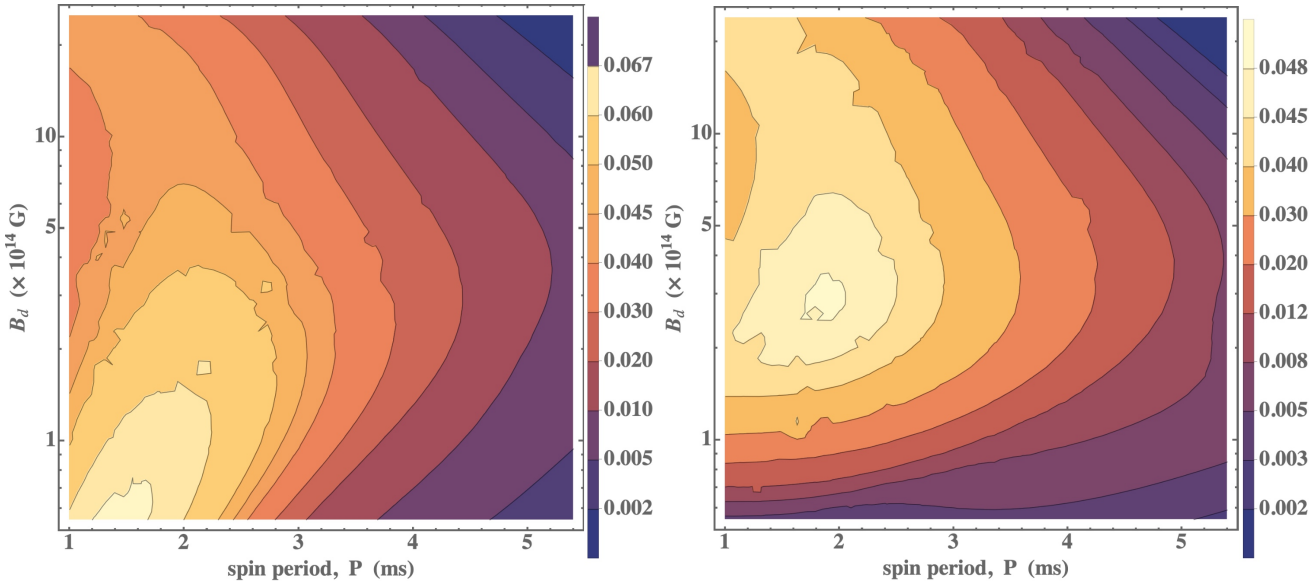

Figure 5. The maximum redshift, $z_{\rm max}$, for detection with ULTRASAT as a function of the magnetar parameters (B_d, P), for fiducial ejecta properties $E_{\rm SN} = 10^{51}$ erg, $M_{\rm SN} = 5M_\odot$. Left panel: only magnetic dipole spindown with no GW emission. Right panel: magnetic dipole spindown plus an efficient GW emission with $\epsilon = 2 \times 10^{-3}$.

fixed value $\epsilon = 2 \times 10^{-3}$ for the NS ellipticity in order to demonstrate the impact of GW emission.

In Figure 5 we show contours of $z_{\rm max}$ as a function of B_d and P for SBOs, with (right panel) and without (left panel) GW emission. We note that our numerical calculations give slightly different light curves and $z_{\rm max}$-values relative to Paper I, even in the absence of GW emission. Thus, the results presented here should be regarded as updates and improvements over our previous calculations. Figure 6 reports the same result for SN light curves, assuming perfect thermalization of $L_{\rm EM}$, with (right panel) and without (left panel) GW emission.

6. Expected Detection Rate

Our results indicate that magnetar-driven SBOs can be detected by ULTRASAT out to $z_{\rm max} \sim 0.045 - 0.06$ (200–280 Mpc) with and without GW emission, respectively, for an extinction $A_{\rm NUV} = 2$ mag and with a strong dependence on the NS B-field, ellipticity, and spin energy. The associated SNe can be detected to larger distances, $z_{\rm max} \sim 0.18 - 0.35$ for the same extinction, and with a similar dependence on the NS parameters.

In order to estimate the expected rate of detections of either SBOs or SNe we average the $z_{\rm max}$-distributions (Figures 5 and 6) over the probability distribution of magnetar parameters in the population. As a result, the number of events per year detectable by ULTRASAT is

$$\dot{N}_{\rm ev} = \int dP dB \int_0^{z_{\rm max}(B,P)} \frac{\mathcal{R}(z)}{(1+z)} \frac{dV}{dz} \mathcal{P}(B)\mathcal{P}(P) dz, \qquad (14)$$

where $\mathcal{R}(z)$ is the comoving volumetric rate of SNe that form a magnetar, which we take to be ∼0.1 of the CCSN rate (B. M. Gaensler et al. 2005; P. Beniamini et al. 2019). The latter is taken from P. Madau & M. Dickinson (2014), while the $(1 + z)$ factor in the denominator accounts for time dilation of the rate. To calculate $dV(z)/dz$ we adopt standard cosmological parameters (e.g., N. Aghanim et al. 2020). The

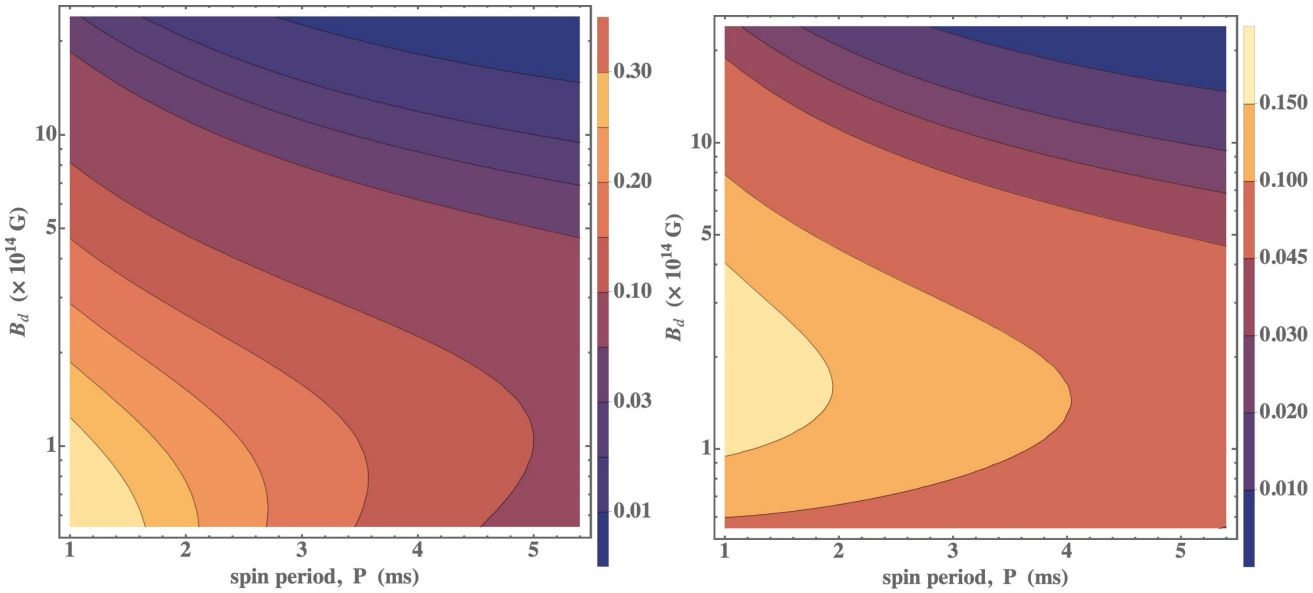

Figure 6. Maximum redshift, $z_{\rm max}$, for detection of magnetar-powered SNe with ULTRASAT as a function of the magnetar parameters (B_d, P), for fiducial ejecta properties $E_{\rm SN} = 10^{51}$ erg, $M_{\rm SN} = 5M_\odot$, and a characteristic $A_{\rm NUV} = 2$ mag. Perfect thermalization of the magnetar spindown power was assumed. Left panel: only magnetic dipole spindown with no GW emission. Right panel: magnetic dipole spindown plus efficient GW emission with $\epsilon = 2 \times 10^{-3}$.

probability distributions of B_d and P in newborn magnetars are currently unknown. Accordingly, we adopt agnostic distributions for each parameter. Since in our scenario magnetars represent the fraction of NSs born with fast rotation, we consider a relatively narrow spin distribution, (1–5) ms (i.e., the remaining 90% of NS are born with slower rotation), with a log-uniform probability, $\mathcal{P}(P) = k_P/P$. Similarly, $\mathcal{P}(B) = k_B/B$ is adopted for the dipole magnetic field strength,[3] with values in the range (0.5–30) $\times$ 10^{14} G.

We restrict our focus to the ULTRASAT high-cadence ($\sim$300 s) survey, with a field of view (FoV) $\sim$204 deg^2 (Y. Shvartzvald et al. 2024), and obtain $\dot{N}_{\rm SBO} \approx (1 - 2.5)$ yr^{-1} with or without GW emission, respectively. While we assumed that $\sim$10% of CCSNe form a magnetar, their detectability in the case without GW is increased over "typical" SBO sources, leading to a larger expected fraction ($\gtrsim$20%) of magnetar-powered SBOs among ULTRASAT detections. For comparison, we also estimated the expected rate of SBO detections by ZTF and obtained a much lower value, $\sim$1 event every $\gtrsim$20 yr.

Similarly, we estimate a detection rate of magnetar-powered SNe $\dot{N}_{\rm SN} \sim 15 - 70$ yr^{-1}, with or without GW emission, respectively, in the case with perfect thermalization of the magnetar spindown power. Accounting for inefficient thermalization, our SNe rate estimate drops to $\sim$10–18 yr^{-1}. Table 1 summarizes our results for different model assumptions.

Table 1
Expected Detection Rate for Magnetar-powered SBOs and SNe with ULTRASAT

ULTRASAT—(230–290) nm						
	SBO		SN			
			Efficient Therm.		Inefficient Therm.	
	no GW	GW	no GW	GW	no GW	GW
Events (yr^{-1})	2.5	1	70	15	18	10

Note. Different assumptions about the emission of GWs are taken into account (the models with GW always adopt a fixed ellipticity $\epsilon = 2 \times 10^{-3}$) from the central engine and the thermalization efficiency of the magnetar MHD wind within the ejecta.

7. Discussion and Conclusions

Our results depicted in Figure 4 provide several insights. A striking feature is the clear separation between the SBO and SN peaks in the bolometric light curves, implying these two components are clearly distinguishable, over an interesting range in parameter space. In the UV band, the SBO peak becomes much less prominent, as a result of the different evolutions of the emission spectra of the SN and the SBO. Taken at face value, this suggests that broadband follow-up observations of ULTRASAT sources will offer the best opportunity for identifying the SBO signature. However, when we account for the inefficient thermalization of the magnetar MHD wind, we find a substantial reduction in the luminosity of the early SN light curve (as in D. Kasen et al. 2016), which strongly favors the emergence of the SBO peak, as illustrated in the right panel of Figure 4.

A second feature is the impact of GW emission on the light curves. We find a relatively small effect in the SBO emission, particularly in the ULTRASAT band. As a consequence, the SBO light curves are expected to be only weakly sensitive to the GW emission by the central engine (although, as stated above, they can pinpoint the presence of a magnetar central engine, particularly for inefficient thermalization of the magnetar MHD wind. On the other hand, we find that GW emission can induce a substantial modification in the UV (and bolometric) light-curve evolution of the SN, with two main implications: first, it clarifies that magnetar central engines do not necessarily produce SLSNe, since part of their spin energy

[3] We repeated our calculation using log-normal distributions and found that our conclusions are robust even with different priors.

could be radiated via GW[4] (see discussion in Paper I and references therein). Furthermore, it opens the possibility to find GW signatures in the SN light curves alone, as their peak luminosities are reduced and their late-time decay can be significantly slower. The latter implies that magnetar-powered SNe with GW emission from the central engine will be brighter, at $t >$ tens of days, than without GW (see L. Xie et al. 2024). A detailed investigation of this important result is postponed for future work and will entail a study of the whole parameter space, in particular disentangling the effects of changing the explosion energy ($E_{\rm SN}$), the ejecta mass ($M_{\rm ej}$), and opacity (κ).

Third, the peak luminosity of SNe in the ULTRASAT band typically exceeds the SBO peak, regardless of the bolometric luminosity. Therefore ULTRASAT may detect several distant magnetar-powered SNe (with/without GWs) missing their early SBO peak, leading to a higher rate of detection of such SNe relative to their SBOs. Accordingly, we estimated the expected detection rate by ULTRASAT of magnetar-powered SNe, adopting the same $A_{\rm NUV} \sim 2$ mag, and obtained $\sim$70 events yr^{-1} in the high-cadence FoV for the case without GW emission and 15 yr^{-1} assuming GW emission with $\epsilon = 2 \times 10^{-3}$. These figures highlight once more the impact that GW emission can have on SN detections. For comparison, we made a conservative estimation of the ZTF detection rate of the same SNe, again adopting $A_{\rm ZTF} \sim 0.6$ mag (A. Zegarelli et al. 2024), and obtained 2 versus 5.5 events yr^{-1} in the case with and without GW, respectively, which is broadly consistent with published results (e.g., Z. H. Chen et al. 2023; P. J. Pessi et al. 2025). We furthermore evaluated the impact of inefficient thermalization of the magnetar spindown power and estimated the corresponding SN detection rate for ULTRASAT, obtaining 10 and 18 events per year with and without GW, respectively.

The possibility to detect magnetar-powered SNe in larger numbers than their SBOs is particularly noteworthy for ULTRASAT. Indeed, the SBO peak occurs typically within the first week (or two, at most) of the explosion and hence can only be well sampled if it occurs within the high-cadence region of the ULTRASAT survey. On the contrary, the SN peaks and their late-time decays—possibly bearing the GW signatures—typically last several tens of days and will thus be well sampled even in the all-sky, low-cadence mode, further contributing to enhancing the detection rate.

Within the estimated GW horizon ($\gtrsim$4 Mpc; see Paper I) for the O5 science run, we expect ULTRASAT to easily detect all magnetar-driven SBOs, hence a multimessenger detection rate $\gtrsim$0.05 yr^{-1}. The 7–8 times larger horizon foreseen for the Einstein Telescope will include the whole Virgo Cluster, and ULTRASAT will be able to detect any SBOs within this distance. Therefore, given a minimum estimated magnetar birth rate of $\sim$0.5 yr^{-1} within 30 Mpc (e.g., L. Stella et al. 2005; S. Dall'Osso et al. 2009), we expect a minimum rate of multimessenger detections of 1 magnetar every 2 yr.

Our results demonstrate that magnetar-driven SBOs and their associated SNe will provide crucial EM triggers for GW searches of long-transients emitted by newly formed magnetars. Besides signaling the start time for the transient GW, the light curves of such events will help constrain the NS spin period and B-field, which in turn determine the GW signal shape. Moreover, as highlighted above, ULTRASAT observations alone of magnetar-powered SNe may offer the unprecedented opportunity to pinpoint the emission of GWs by the central engine, informing direct GW searches in unique ways.

[4] Strong GW emission ($\epsilon > 10^{-3}$) can reduce the SN peak luminosity by a factor $\sim$2–3 for a wide parameter range. In our simple calculation $<1/5$ of magnetars have a sufficiently fast spin (period $\lesssim$3 ms) and strong B-field ($>3 \times 10^{14}$ G) to power an SLSN.

Acknowledgments

S.D. acknowledges financial support from the grant ASI-INAF 2023-17-HH.

ORCID iDs

Simone Dall'Osso https://orcid.org/0000-0003-4366-8265
Dafne Guetta https://orcid.org/0000-0002-7349-1109

References

Aghanim, N., Akrami, Y., Ashdown, M., et al. 2020, A&A, 641, A6
Beniamini, P., Hotokezaka, K., van der Horst, A., & Kouveliotou, C. 2019, MNRAS, 487, 1426
Chen, Z. H., Yan, L., Kangas, T., et al. 2023, ApJ, 943, 42
Chevalier, R. A. 2005, ApJ, 619, 839
Chevalier, R. A., & Soker, N. 1989, ApJ, 341, 867
Corsi, A., & Mészáros, P. 2009, ApJ, 702, 1171
Cutler, C. 2002, PhRvD, 66, 084025
Dall'Osso, S., Giacomazzo, B., Perna, R., & Stella, L. 2015, ApJ, 798, 25
Dall'Osso, S., Shore, S. N., & Stella, L. 2009, MNRAS, 398, 1869
Dall'Osso, S., & Stella, L. 2022, in Millisecond Pulsars, ed. S. Bhattacharyya, A. Papitto, & D. Bhattacharya (Cham: Springer), 245
Dall'Osso, S., Stella, L., & Palomba, C. 2018, MNRAS, 480, 1353
Duncan, R. C., & Thompson, C. 1992, ApJ, 392, L9
Ferrario, L., & Wickramasinghe, D. 2006, MNRAS, 367, 1323
Gaensler, B. M., McClure-Griffiths, N. M., Oey, M. S., et al. 2005, ApJL, 620, L95
Gal-Yam, A. 2019, ARA&A, 57, 305
Ganot, N., Gal-Yam, A., Ofek, E. O., et al. 2016, ApJ, 820, 57
Gao, H., Zhang, B., & Lü, H.-J. 2016, PhRvD, 93, 044065
Gompertz, B. P., O'Brien, P. T., & Wynn, G. A. 2014, MNRAS, 438, 240
Gompertz, B. P., van der Horst, A. J., O'Brien, P. T., Wynn, G. A., & Wiersema, K. 2015, MNRAS, 448, 629
Gottlieb, O., & Metzger, B. D. 2024, ApJL, 974, L9
Greiner, J., Mazzali, P. A., Kann, D. A., et al. 2015, Natur, 523, 189
Kasen, D., & Bildsten, L. 2010, ApJ, 717, 245
Kasen, D., Metzger, B. D., & Bildsten, L. 2016, ApJ, 821, 36
Kulkarni, S., Harrison, F. A., Grefenstette, B. W., et al. 2021, arXiv:2111.15608
Lamb, G. P., Baxter, T., Omand, C. M. B., et al. 2025, MNRAS, 540, 2727
Lander, S., & Jones, D. 2020, MNRAS, 494, 4838
Leloudas, G., Chatzopoulos, E., Dilday, B., et al. 2012, A&A, 541, A129
Liu, L.-D., Gao, H., Wang, X.-F., & Yang, S. 2021, ApJ, 911, 142
Madau, P., & Dickinson, M. 2014, ARA&A, 52, 415
Menon, S. S., Guetta, D., & Dall'Osso, S. 2023, ApJ, 955, 12
Metzger, B. D., & Piro, A. L. 2014, MNRAS, 439, 3916
Moriya, T. J. 2024, arXiv:2407.12302
Nicholl, M., Smartt, S. J., Jerkstrand, A., et al. 2015, MNRAS, 452, 3869
Pessi, P. J., Lunnan, R., Sollerman, J., et al. 2025, A&A, 695, A142
Raynaud, R., Guilet, J., Janka, H.-T., & Gastine, T. 2020, SciA, 6, eaay2732
Sagiv, I., Gal-Yam, A., Ofek, E., et al. 2014, AJ, 147, 79
Shvartzvald, Y., Waxman, E., Gal-Yam, A., et al. 2024, ApJ, 964, 74
Stella, L., Dall'Osso, S., Israel, G., & Vecchio, A. 2005, ApJ, 634, L165
Sun, H., Wang, C. W., Yang, J., et al. 2025, NSRev, 12, nwae401
Sur, A., & Haskell, B. 2021, MNRAS, 502, 4680
Thompson, C., & Duncan, R. C. 1993, ApJ, 408, 194
Usov, V. V. 1992, Natur, 357, 472
Vink, J. 2008, AdSpR, 41, 503
Vink, J., & Kuiper, L. 2006, MNRAS: Letters, 370, L14
Xie, L., Gong, H.-Y., Li, L., Wei, D.-M., & Han, J. L. 2024, ApJ, 967, 160
Zegarelli, A., Guetta, D., Celli, S., et al. 2024, A&A, 690, A187
Zhang, B., & Mészáros, P. 2001, ApJL, 552, L35